Jordan Journal of Civil Engineering, Volume **18**, No. **2**, **2024**
DOI: https://doi.org/10.14525/JJCE.v18i2.10

Jordan Journal of Civil Engineering

Journal homepage: https://jjce.just.edu.jo

Wind Pressure of Low-rise Buildings Based on Wind-tunnel Numerical-simulation Test

Ding Huiqi [1)*]

[1)] *Changsha University of Science & Technology, Changsha 410114, China.*
** Correspondence Author. E-Mail: DHQ2023625@163.com*

ARTICLE INFO

Article History:
Received: 29/9/2023
Accepted: 10/3/2024

ABSTRACT

Based on the numerical-simulation test data from the wind tunnel, the wind-pressure characteristics of low-rise buildings with gable roofs are examined and compared to standard values under different roof slopes, eave heights and terrains. To further investigate the underlying mechanisms of variation, a numerical-simulation study was conducted for selected conditions. The results indicate that when the roof slope is less than 3:12, the negative value of the shape coefficient for the windward roof of the building can reach up to -0.89, far exceeding the code value of -0.5. It is suggested that when the slope is not larger than 3:12, the shape coefficient for the windward roof should be -0.9 and the coefficient for the leeward roof should be determined through linear interpolation within the range from -0.4 to -0.75 based on the roof's slope size. With the increase of eave height and the decrease of ground roughness, the vortex intensity of the roof and the leeward surface increases and the area proportion of high negative pressure area in the vortex influence range increases. Thus, the negative value of the shape coefficient for the roof and the leeward surface becomes larger, which is higher than the code value. It is proposed that under an eave height of 12 m, the shape coefficient for the windward roof should be -0.95. Meanwhile, those of the leeward roof, leeward surface and sidewall 2 should be -0.6 under open terrain.

Keywords: Low-rise buildings, Wind-tunnel test, Wind load, Shape coefficient, Numerical simulation.

INTRODUCTION

More than a half of the globally occurring economic losses related to weather can be attributed to strong wind events (Yang et al., 2018; Huang & Wang, 2008). Wind disasters have had a significant impact on the economic development of human society and have resulted in extensive structural damage. Among these structures, low-rise buildings are the most affected (Hajra & Dalui, 2016). Therefore, it is essential to incorporate wind-resistant design in the construction of low-rise buildings. Wind-tunnel testing is widely recognized as a more accurate method for assessing structural wind loads. Researchers, such as Yang et al. (2008), Yang et al. (2013) and Prasad et al. (2009), began using wind-tunnel tests to study wind pressures on buildings and applied the test results to estimate wind loads on low-rise structures, thus laying the foundation for the development of related design codes. Cheon et al. (2023) investigated the effects of roof slope and span on

the local pressure coefficients of gable roofs through wind-tunnel testing and found that the wind-pressure values exceeded the identified code values under certain conditions. Tariq et al. (2023) studied the wind-pressure characteristics of low-rise buildings in different wind directions using wind-tunnel tests and visualized experiments and concluded that a wind-direction angle of 0° is not necessarily the most critical scenario. Irtaza et al. (2015) discovered that the wind pressure on low-rise buildings is also influenced by the surrounding environment and roof slope. Ginger et al. (2003) studied wind loads on low-rise buildings with steep roof slopes. Gu et al. (2010) investigated the wind-pressure distribution on the roofs of low-rise buildings. They pointed out that the wind direction not only alters the distribution of roof pressures, but also affects the influence of other parameters on roof pressures. Akon and Kopp (2016) conducted wind-tunnel tests and found that increased turbulence intensity in the incoming flow leads to changes in the wind-pressure distribution on the roofs of low-rise buildings. In recent years, Guo et al. (2021), Wang and Kopp (2021) and Kozmar (2020) have studied the effects of small-scale vortices, horseshoe vortices and conical vortices around building models on the mean pressure coefficient. They found that factors, such as wind direction, building geometry and terrain, influence the pressure distribution by affecting the intensity of vortices around the buildings and the size of their influence regions. The computational fluid dynamics (CFD) method is a method that utilizes computers for numerical simulation and analysis of fluid-dynamics problems based on numerical methods and mathematical models and, through discretization of fluid-dynamics equations, simulates and analyzes phenomena, such as fluid motion, heat transfer and mass transfer. With the growth of high-performance computing resources, numerical-simulation methods, such as Reynolds-averaged Navier-Stokes (RANS) and Large-Eddy Simulation (LES), have been applied in the study of building wind pressures and the analysis of surrounding flow fields (Agrawal et al., 2022; Xing et al., 2018). The RANS method is a classic mean-flow equation method that decomposes flow variables into mean values and pulsating components by performing time and vortex averaging on flow variables in both time and space. The LES method is a direct simulation of large-vortex structures with the highest energy in turbulence while filtering out small-scale-vortex structures. This method filters the flow variables in space and decomposes them into a large-scale turbulent part and a small-scale-turbulent part. Kobayashi et al. (2022). utilized CFD to investigate the influence of building form on surface-pressure distribution. Abdelfatah et al. (2022) studied the flow-field distribution around low-rise residential buildings. They found that oblique winds lead to high suction on building surfaces, resulting in damage to building envelopes and ancillary structures.

In summary, the characteristics of building wind loads are complex and influenced by various factors, such as wind direction, roof slope, building dimensions and surrounding terrain. However, in China's "Code for Loadings in Building Structures" (GB 50009-2012), only corresponding shape coefficients are provided for different building types, with no mention of other influencing factors. Therefore, it is necessary to investigate the applicability of these coefficients and consider further refinement. Based on wind-tunnel numerical-simulation test data and numerical simulations, this study aims to explore the rationality of coefficient values in design codes and propose more refined values. Firstly, an overview of the wind-tunnel test data and parameters utilized in the numerical simulations conducted at the University of Western Ontario (UWO) is provided. Subsequently, the effects of factors, such as wind-direction angle, roof slope, eave height and terrain, on wind-pressure characteristics are analyzed and compared with the values specified in the design codes. Finally, relevant conclusions are drawn.

Experimental Data and Parameter Settings in Numerical Simulation

Experimental Data

The experimental data was obtained from the Boundary Layer Wind Tunnel Laboratory at the UWO using the National Institute of Standards and Technology (NIST) aerodynamic database (Chinese Ministry of Housing and Urban-Rural Development, 2012; Ho et al., 2005). The model used was a scaled-down version of a low-rise building with a scale ratio of 1:100. The experiments considered two types of terrains: open and sub-urban, with roughness lengths of 0.03m and 0.3m, respectively, corresponding to ground-roughness categories B and C specified in the design code. The prototype of the building had a plan dimension of 38.2 m × 24.4 m and included variations

in roof slope, eave height and wind-direction angle. The sampling frequency of the experiments was 500 Hz, with a sampling duration of 100 seconds. When the roof slope is 1/4:12, the eaves heights are 3.66m, 5.49m, 7.32m, 9.75m and 12.20m respectively, with wind directions ranging from 0° to 90° and intervals of 5°. When the roof slope is 1:12, the eave heights are 4.88m, 7.32m, 9.75m and 12.20m respectively, with wind directions ranging from 0° to 90° and intervals of 5°. When the roof slope is 3:12, the eave heights are 4.88m, 7.32m, 9.75m and 12.20m, respectively, with wind directions ranging from 0° to 90° and intervals of 5°. When the roof slope is 6:12, the eave heights are 3.66m, 7.32m and 12.20m, respectively, with wind angles ranging from 0° to 90° and intervals of 5° (Ho et al., 2003; Ho et al., 2003).

Define the wind pressure and set the pressure on the force surface to be positive and the suction to be negative. A reference point is usually chosen as a point with known static and total pressure values for comparison and calculation of wind pressure at other locations. It can be anywhere on the surface of a building or in an air-flow field. By setting the static pressure at that reference point to zero and measuring the total pressure at that point, the wind pressure at each measurement point relative to the reference point can be calculated (Ho et al., 2003; Ho et al., 2003). The wind-pressure coefficient C_{Pi} of the measuring point is calculated as follows:

$$C_{P_i} = \frac{P_i - P_\infty}{P_0 - P_\infty} \quad (1)$$

In Formula (1), P_i is the pressure acting on the measuring point i, P_0 and P_∞ are the total pressure and static pressure, respectively, at the reference height of the test. According to the time history of the wind pressure coefficient at the measuring point $\{C_{Pi}(t_j)\}$ $(j = 1,2,\cdots,n)$, the average wind pressure coefficient $C_{Pmean,i}$ is calculated as follows:

$$C_{Pmean,i} = \frac{\sum_{j=1}^{n} C_{P_i}(t_j)}{n} \quad (2)$$

n in Formula (2) is the total number of samples. The wind load at each measuring point of the building can be calculated according to the following formula:

$$F_i = C_{Pmean,i} w_Z A_i \quad (3)$$

In Formula (3), w_Z is the wind pressure at the reference height of the test and A_i is the area (m^2) corresponding to the pressure-measurement point i.

The shape coefficient of wind load refers to the ratio of the average pressure or suction caused by wind acting on a certain area of the building surface to the velocity pressure of the incoming wind. The local wind load-shape coefficient of each pressure-measuring point is equal to the average wind-pressure coefficient and the overall shape coefficient is the result of the weighted average wind-pressure coefficient of each point, which is calculated using Formula (5).

$$\mu_{si} = C_{Pmean,i} \quad (4)$$

$$\mu_s = \frac{\sum \mu_{si} A_i}{A} = \frac{\sum \mu_{si} A_i}{\sum A_i} \quad (5)$$

In Formula (5), μ_{si} is the body-shape coefficient of the i^{th} measuring point and A (m^2) is the total area or the total windward area of the calculated surface.

The standard value of wind load acting on the building surface at the height z specified in the code is calculated as follows (Ming-Fei et al., 2011):

$$w_z = \beta_z \mu_s \mu_z w_0 \quad (6)$$

where: β_z is the wind-vibration coefficient at the height z. Taking β_z = 1, μ_s is the shape coefficient of the wind-load point, μ_z is the height-variation factor of wind pressure and w_0 is the basic wind pressure.

Parameter Settings in Numerical Simulation

To investigate the flow characteristics around low-rise buildings as the geometric properties of the building models vary, computational fluid dynamics (CFD) numerical imitations were accomplished on wind-tunnel test models. The advantages of the CFD algorithm in the analysis of low-rise buildings are: (1) Fine simulation: CFD can accurately model the geometric characteristics of complex-building models, including building shape, wall characteristics and flow characteristics, such as airflow velocity, pressure distribution and turbulence structure. (2) Flexibility and customizability: The CFD algorithm allows for the selection of different boundary conditions and model parameters based on the specific needs of the problem. This allows for flexible adjustment of simulation settings during the analysis process to meet specific research objectives. (3) Cost and time savings: Compared to traditional experimental methods, CFD simulation can significantly reduce costs and time. Through simulation calculations, we can

quickly obtain the flow-field distribution under multiple operating conditions without the need for actual physical testing and experimentation. (4) Parameterization research: The CFD algorithm can effectively support parameterization research. By changing the geometric characteristics, material properties and other parameters of the building model, the impact of different design decisions on flow characteristics can be quickly evaluated to optimize the building design.

The numerical simulation utilized the SST k-ω turbulence model (Menter et al., 2003) and simulated the flow of an incompressible Newtonian fluid in three dimensions. The steady-state velocity and pressure were solved using the SIMPLE algorithm, with a convergence criterion set at 10^{-6}. The SIMPLE algorithm is a commonly used CFD algorithm for solving steady-state or non-stationary incompressible fluid-flow problems. The main idea is to divide the coupling of velocity and pressure into two steps for solving. The advantage of the SIMPLE algorithm is that it has good numerical stability and exhibits good convergence for most incompressible fluid-flow problems. In addition, the SIMPLE algorithm can effectively handle the pressure-velocity coupling problem in the flow field and strike a balance between computational efficiency and accuracy.

A slope of 1/4:12 means an increase of 1 foot for each horizontal distance and a 1/4 foot increase in roof height. This slope is usually used in areas with lower rainfall and mild climate conditions to ensure smooth discharge of precipitation. An eave height of 12.2m is chosen based on the purpose, functional requirements, limitations of the building plan and the needs of the surrounding environment of the building. For the reference configuration, based on a building model with a roof slope of 1/4:12 and an eave height of 12.2 m, a sensitivity analysis of grid resolution was conducted using three different grid configurations: coarse (3.494 million cells), medium (4.864 million cells) and fine (7.312 million cells). The grid resolution was achieved by varying the growth rate while maintaining the first cell height at 4×10^{-5}. Grid-independence tests were performed on the three grid configurations and the numerical-simulation results were compared with wind-tunnel test data. It can be observed that the differences between the fine and medium grids are relatively small, while the differences between the coarse and medium grids are rather big. Considering the trade-off between computation precision, correctness and expense, the medium grid was selected for more evaluation, as follows:

1. Shape Coefficient of Low-rise Buildings

The shape coefficient of a building structure is a fundamental parameter for calculating structural wind loads. Next, considering the variation of wind direction, we will explore the influence of parameters, such as roof slope, eave height and terrain, on the shape coefficients of surfaces in low-rise buildings.

2. Roof Slope

Four distinct models, each with a unique roof slope, were selected to thoroughly investigate the alterations in wind-pressure distribution characteristics. This analysis considered an open terrain and a ridge height of 12.2 m, while also accounting for diverse roof slopes. Figure 1 displays the shape-coefficient values for each wall surface, featuring roof slopes ranging from 1/4:12 to 6:12. Given the maximum slope of 6:12, subsequent analysis will be confined to roof angles within 30°, focusing primarily on the most relevant cases.

The standards differentiate the values of the shape coefficient for the windward roof based on roof slopes of 15°, 30° and 60°. Among these, roof slopes of 3:12 and 6:12 are approximately close to 15° and 30°, respectively. From Figure 1(a), it can be observed that for roof slopes within 15°; namely, 1/4:12, 1:12 and 3:12, the negative shape coefficients for the windward roof exceed the specified value of -0.6 within 0° to 30° wind-direction range. The windward roof experiences significant wind suction. Specifically, for a roof slope of 1:12, the shape coefficient at a 0° wind direction is -0.89, which is 1.48 times the value specified in the standards. Analyzing Figure 1(b), it can be seen that for leeward roofs, the shape coefficients of roof slopes at 6:12, 3:12, 1:12 and 1/4:12 all exceed the specified value of -0.5 at 75° wind direction. The shape coefficient is highest at 0° wind direction. Analyzing Figure 1(c), it can be seen that for the windward side, as the wind-direction angle increases, the shape coefficients of roof slopes at 6:12, 3:12, 1:12 and 1/4:12 show a continuous decreasing trend, all of which being less than the specified value of 0.8. Analyzing Figure 1(d), it can be seen that for the leeward side, as the wind-direction angle increases, the shape coefficients of roof slopes at 6:12, 3:12, 1:12 and 1/4:12 all show a first decreasing and then increasing trend. The shape coefficients of roof slopes at 6:12 and

3:12 do not exceed the specified value, while the shape coefficients of roof slopes at 1:12 and 1/4:12 exceed the specified value of -0.5 within a certain angle. Analyzing Figure 1(e), it can be seen that for page wall 1, as the wind-direction angle increases, the shape coefficients of roof slopes at 6:12, 3:12, 1:12 and 1/4:12 all show an upward trend and are all higher than the specified value of -0.7. Analyzing Figure 1(f), it can be seen that for page wall 2, as the wind-direction angle increases, the shape coefficients of roof slopes at 6:12, 3:12, 1:12 and 1/4:12 all show a fluctuating upward trend, all of which being higher than the specified value of -0.7.

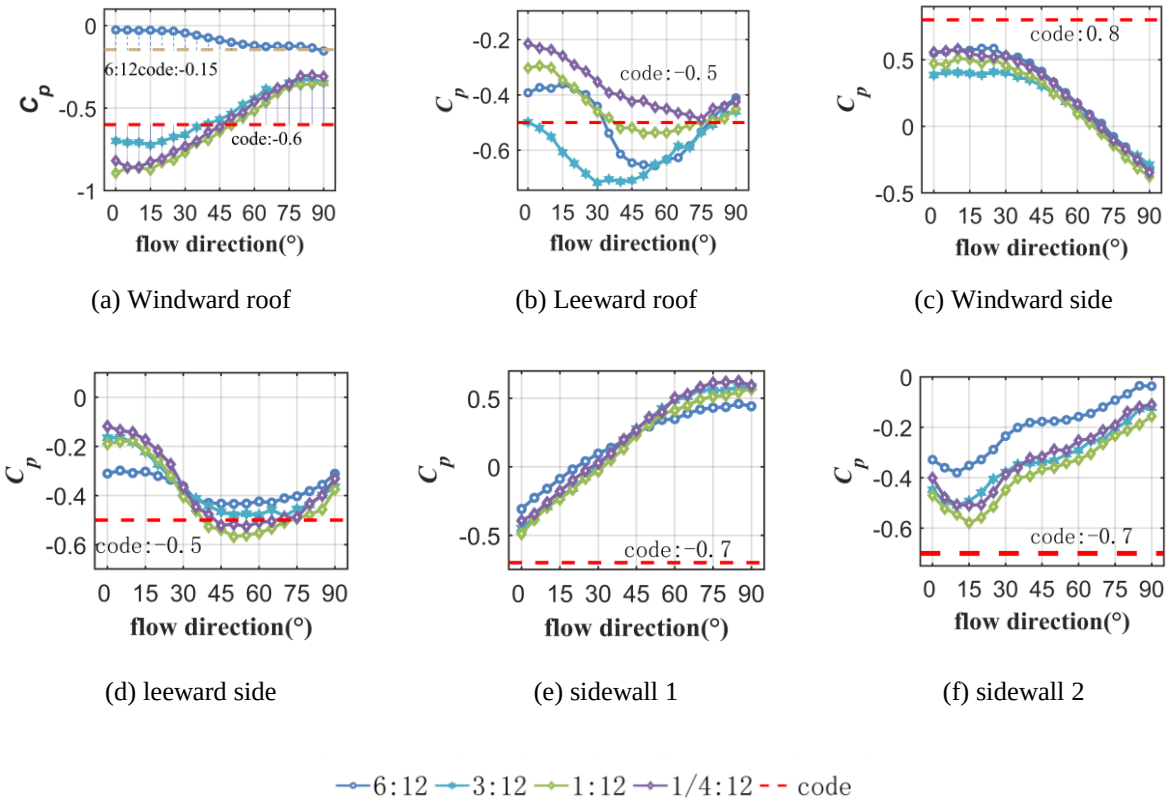

(a) Windward roof (b) Leeward roof (c) Windward side

(d) leeward side (e) sidewall 1 (f) sidewall 2

Figure (1): Shape coefficient of each wall at different roof slopes

From Figures 2(a) and 2(b), it can be observed that as the roof slope increases from 1:12 to 3:12, the high negative-pressure zone of the separation zone near the windward leading edge gradually moves closer to the ridge and the length of reattachment decreases. According to the standards, for buildings with roof slopes below 15°, a uniform shape coefficient of -0.6 is recommended for the windward roof. Considering models with roof slopes within 15°, the values of the shape coefficient for the windward roof do not differ significantly for different wind directions. However, under 0° wind direction, the negative shape coefficient for the windward roof exceeds the specified value. As the roof slope increases to 6:12, the negative shape coefficient for the windward roof significantly decreases and remains within the limits specified in the standards. From Figure 2(c), it can be observed that as the roof slope increases from 3:12 to 6:12, the range and intensity of the separation vortex at the windward leading edge decrease. The negative-pressure area on the roof decreases and a large area of positive pressure appears, resulting in a significant reduction in the negative shape coefficient.

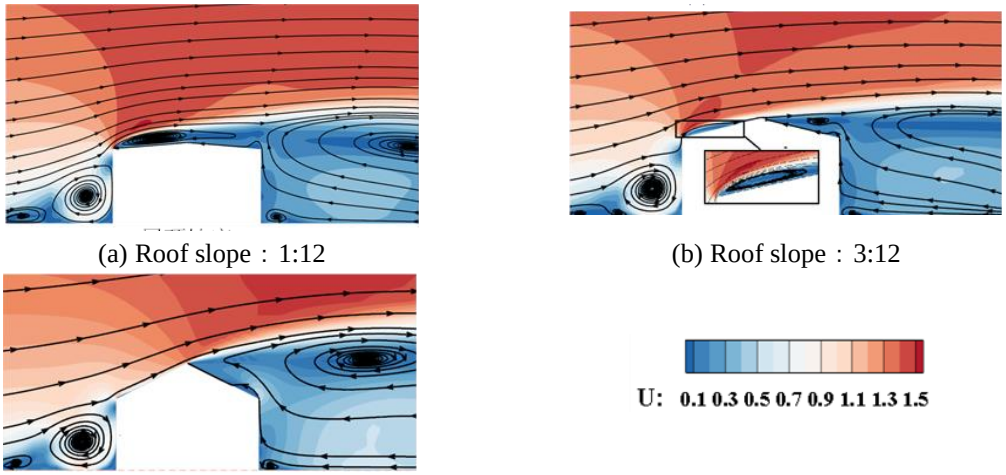

(a) Roof slope：1:12

(b) Roof slope：3:12

(c) Roof slope：6:12

Figure (2): Surrounding wind field of building at 0° flow direction

Analyzing a typical vortex form of characteristic turbulence, it can be seen that when the wind passes through a building, a phenomenon called “a conical vortex” is formed. A conical vortex refers to a pair of rotating vortices formed when the wind passes through buildings or other obstacles at a certain speed, causing the airflow to separate and form. One vortex will detach from the building and form a negative-pressure area behind it, while the other vortex will attach to the building to form a positive-pressure area. These two vortices will alternate and move backward from both sides of the building. Conical vortices are a common phenomenon for high-rise buildings, causing oscillations and vibrations, which may lead to fatigue failure of the building structure.

Figure 3 shows that for roof slopes within 15°, considering the most unfavorable wind conditions from all wind directions tested in the wind tunnel, the shape coefficient for the windward roof approaches -0.9, which is considerably lower than the specified value of -0.6, indicating a higher level of risk. As the roof slope increases from 3:12 to 6:12, the negative shape coefficient for the windward roof significantly decreases. Figure 3 shows that for a roof slope of 6:12, the shape coefficient for the windward roof is equal to the specified value of -0.15. Based on the wind-tunnel test results, a shape coefficient of -0.9 is recommended for roof slopes within 15° on the windward side. For a roof slope of 30°, the recommended value is 0.0, as specified in the standards. For roof slopes between 15° and 30°, considering the limited data on different slope conditions, it is advisable to use linear interpolation based on the standard guidelines. The shape coefficient for the windward roof can be determined by linear interpolation within the range of -0.9 to 0.0.

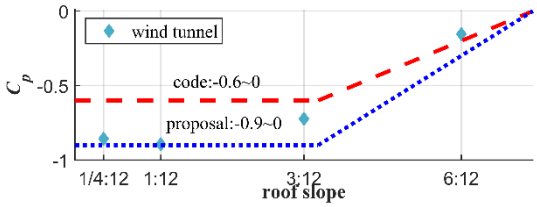

Figure (3): Recommended value of shape coefficient of windward roof

By considering the wind-pressure coefficient distribution in Figure 4(b), it can be noted that for a roof slope of 3:12, the incoming flow separates near the leading edge of the windward roof and reattaches near the ridge. A conical vortex is formed on the roof, with an enhanced negative-pressure region within the flow-separation area. The maximum negative pressure is formed at the windward edge corner and the negative pressure decreases along the direction of the conical vortex until it reaches the roof edge. Locations, such as the roof corners and roof edges, exhibit the highest negative wind-pressure coefficients, leading to an increase in the shape coefficient for the leeward roof as the roof slope does not exceed 3:12; a higher roof slope results in a higher degree of separation and reattachment. However, when the slope increases to 6:12, the incoming flow separates at the ridge and does not reattach to the leeward roof. Consequently, a larger negative shape coefficient is observed, indicating significant suction.

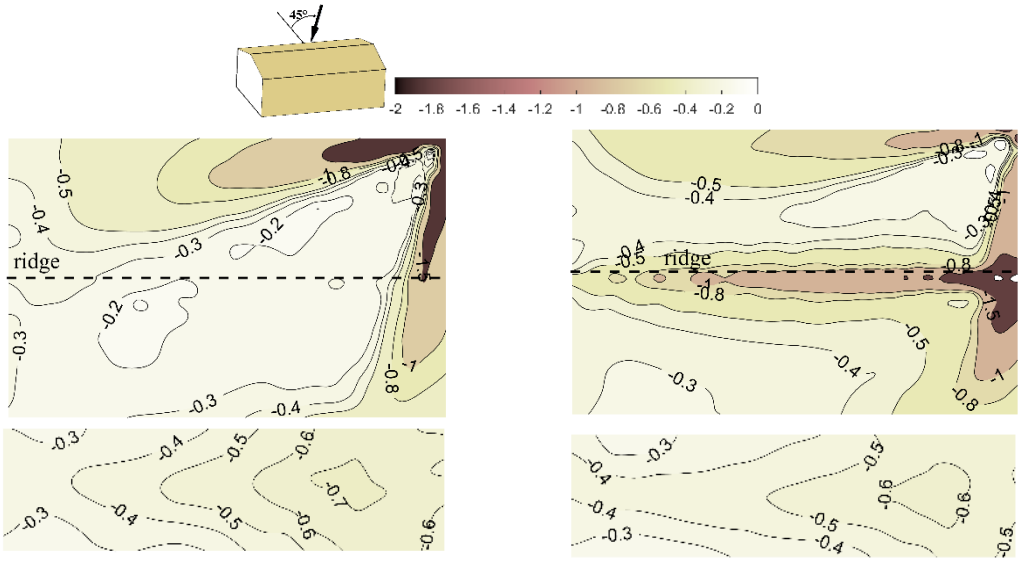

(a) Roof slope: 1/4:12; wind-direction angle: 45° (b) Roof slope: 3:12; wind-direction angle: 45°

Figure (4): Distribution diagram of mean wind-pressure coefficient of the roof and leeward surface

Figure 5(a) illustrates the most unfavorable values of the shape coefficient for the leeward roof, considering different wind directions for various roof slopes. As the roof slope increases, the negative values of the shape coefficient initially increase and then decrease. Therefore, it is recommended that when the roof slope ranges from 0 to 15°, the shape coefficient for the leeward roof should be linearly interpolated within the range from -0.4 to -0.75. For roof slopes ranging from 15° to 30°, a uniform value of -0.75 is recommended.

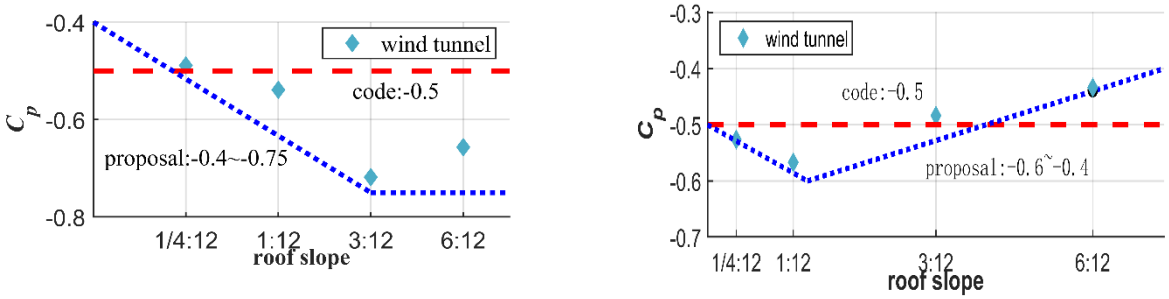

(a) Recommended values of shape coefficient for leeward roof (d) Recommended values of shape coefficient on the leeward surface

Figure (5): Recommended value of shape coefficient for leeward roof and coefficient on the leeward surface

As shown in Figure 5(b), the negative values of the shape coefficient for the leeward facade increase and then decrease as the roof slope increases, with the maximum negative value occurring at a roof slope of 1:12. Therefore, when the roof slope increases from 0 to 5° (close to a slope of 1:12), the shape coefficient for the leeward facade can be interpolated between -0.5 and -0.6. When the roof slope increases from 5° to 30°, the shape coefficient for the leeward facade can be linearly interpolated between -0.6 and -0.4.

By analyzing the wind-pressure distribution on building sidewall 2 under different roof slopes, the maximum suction is observed near the sidewall and roof-ridge junction. For roof-slopes below 15°, the shape coefficient of sidewall 2 shows little variation with slope. However, as the slope increases from 3:12 to 6:12, the maximum negative pressure decreases and the proportion of the area with negative pressure below -0.5 decreases on the entire wall surface. Consequently, the negative values of the shape-coefficient for sidewall 2 decrease. The shape coefficient values for the windward facade and sidewall 1 are similar for different roof

slopes and do not exceed the code-prescribed values. Therefore, further discussion on these aspects is not necessary.

In conclusion, increasing the roof slope primarily affects the shape coefficients of the roof, leeward facade and sidewall 2. For the windward roof, the overall negative values of the shape coefficient decrease as the slope increases, indicating that the prescribed values in the code are conservative for slopes up to 15°. For the leeward roof and leeward facade, the negative values of the shape coefficient initially increase and then decrease with increasing slope. The code does not account for the influence of slope and within slopes up to 30°, there is a potential risk associated with the prescribed values. For slopes up to 15°, the shape coefficient of sidewall 2 shows little variation with slope, but as the slope continues to increase, the negative values of the shape coefficient decrease.

Eave Height

By selecting an open-terrain condition, a slope ratio of 1:12 and varying eave heights, a model study was conducted to investigate the influence of eave height on the form-factor coefficient of each building surface. The shape coefficients of each wall at different roof heights are shown in Figure 6. From Figure 6(a), it can be observed that as the eave height increases, the corresponding negative values of the form-factor coefficient for the windward roof of the buildings also increase. For low-rise buildings with eave heights exceeding 4.88m, the negative values of the form-factor coefficient for the windward roof consistently exceed the specified value of -0.6.

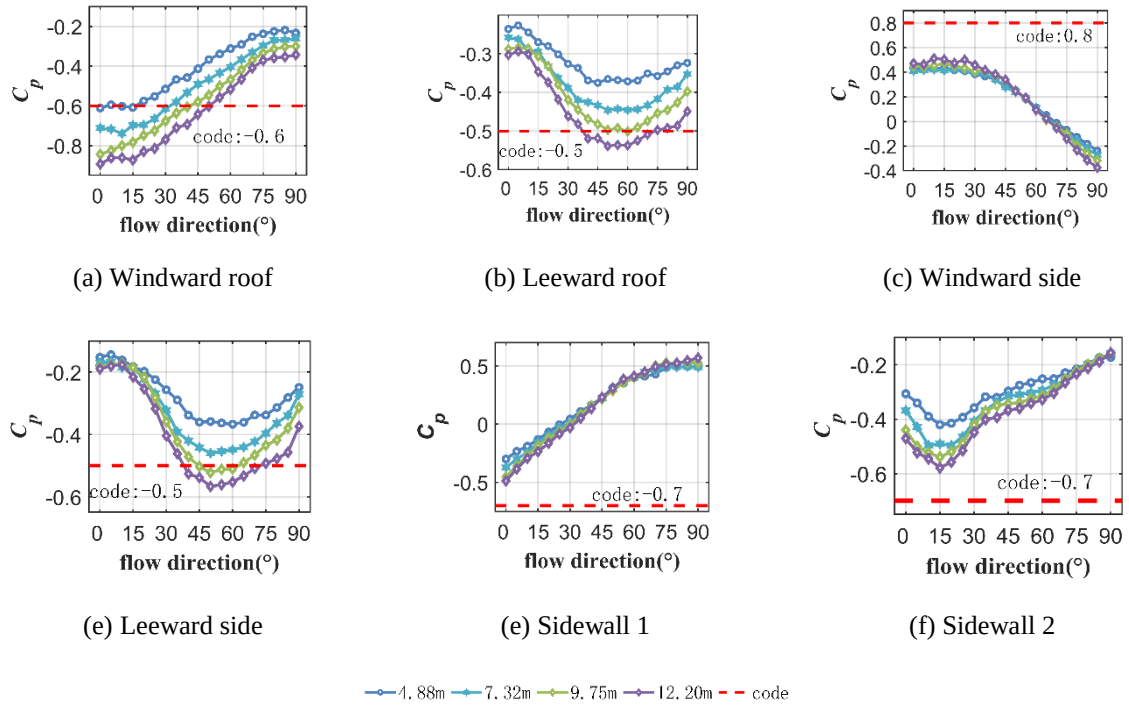

(a) Windward roof (b) Leeward roof (c) Windward side

(e) Leeward side (e) Sidewall 1 (f) Sidewall 2

Figure (6): Shape coefficient of each wall at different roof heights

When the incoming airflow separates from the leading edge of the windward roof, suction is generated. The negative-pressure regions associated with separation are similar across different heights, but the subsequent airflow reduces the negative-pressure experienced by the roof. As the eave height increases, the length of the attached-flow region also increases and the range of the high negative-pressure region caused by separation expands. This results in an overall increase in the negative pressure experienced by the roof.

For the leeward roof, leeward surface and sidewall 2, the negative values of the form-factor coefficient also increase with the increase in height. For buildings with heights exceeding 7.32 m, both the leeward roof and leeward surface exhibit form-factor coefficient negative values that surpass the specified limit. From Figure 7, it

can be observed that at a wind-direction angle of 75°, as the eave height increases, the strength and affected area of the high negative-pressure region caused by the conical vortex on the leeward roof increase, increasing the negative values of the form-factor coefficient. The negative values of the high-pressure region on the leeward surface also increase with the increase in eave height, indicating that under the scenario of increased eave height, the intensity of the wake vortex on the leeward surface increases, leading to an increase in the negative values of the form-factor coefficient.

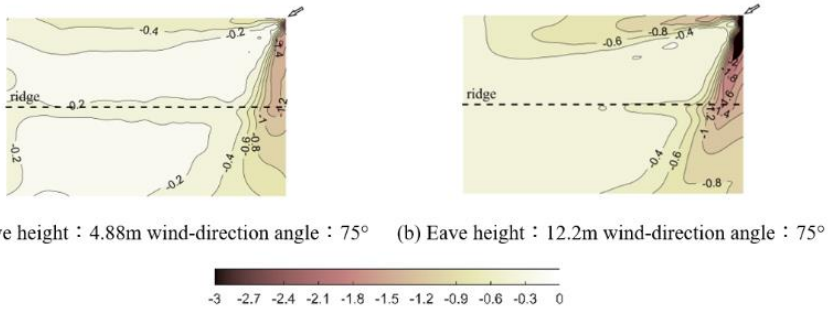

(a) Eave height：4.88m wind-direction angle：75° (b) Eave height：12.2m wind-direction angle：75°

Figure (7): Wind-pressure coefficient distribution map of a leeward roof with different eave heights

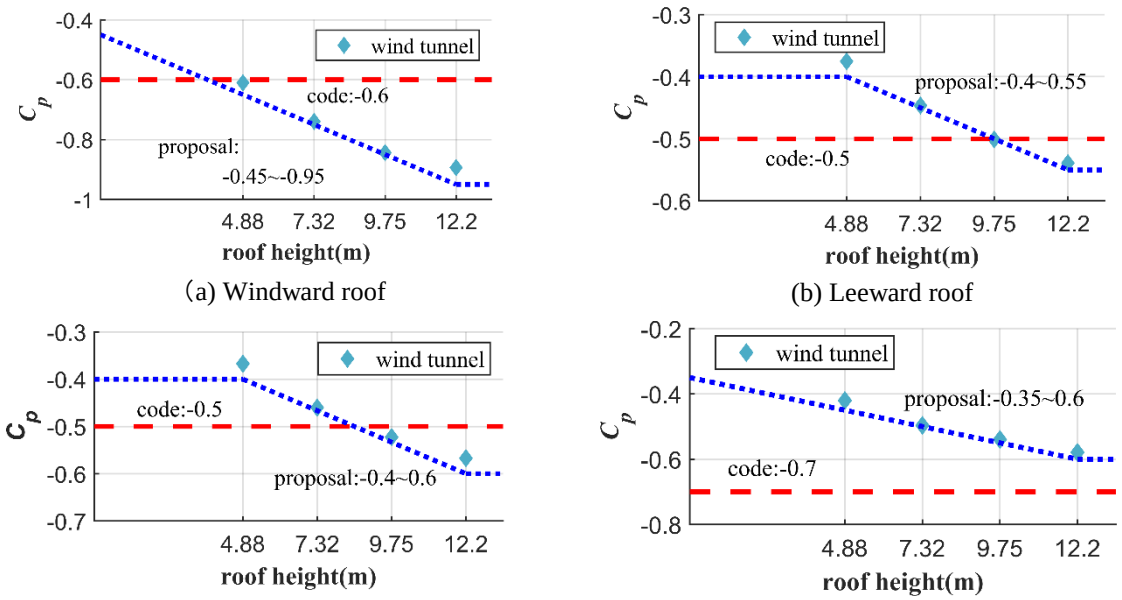

(a) Windward roof (b) Leeward roof

(c) Leeward side (d) Sidewall 2

Figure 8: Recommended values of shape coefficient with different eave heights

The maximum suction occurs in the corner region near the windward surface's top. Increasing the eave height leads to a larger proportion of the overall area being occupied by the high negative-pressure region, increasing the negative values of the form-factor coefficient. For different eave heights, the form-factor coefficient values for the windward surface and sidewall 1 of the building model are similar, thus not warranting further discussion.

It can be concluded that with the increase in eave height, the intensity and influence range of vortices around the building gradually increase. This leads to an increasing trend in wind pressure on various surfaces, particularly on the roof, leeward surface and sidewall 2. As shown in Figure 8, as the eave height increases, the negative values of the form-factor coefficient for the roof and wall surfaces also increase, exceeding the specified values.

The experimental results recommend determining the form-factor coefficient values for the windward roof as a linear interpolation between -0.45 and -0.95 when the eave height is less than or equal to 12.2 m. For the

leeward roof, a uniform form-factor coefficient of -0.4 can be used when the eave height is less than 4.88 m and from 4.88 m to 12.2 m, the form-factor coefficient can be linearly interpolated between -0.4 and -0.55. Similarly, for the leeward surface, a form-factor coefficient of -0.4 can be used when the eave height is less than 4.88m and from 4.88 m to 12.2 m, the form-factor coefficient can be linearly interpolated between -0.4 and -0.6. For sidewall 2, the form-factor coefficient can be determined through linear interpolation between -0.35 and -0.6 when the eave height is less than or equal to 12.2 m.

Topography

We selected a slope ratio of 1:12 and a height of 12.2m and built relevant models considering both open and sub-urban terrain types to determine the impact of terrain on the shape coefficient of each building surface. Open terrain usually refers to a flat, vast terrain without obvious undulations or obstacles. This type of terrain typically occurs in areas, such as great plains, grasslands and deserts, characterized by flat terrain, open views and few or no obstacles, such as hills and rivers. The sub-urban terrain refers to the terrain of the urban suburbs, usually including natural terrain, such as hills, mountains, rivers and artificial buildings, such as residential areas, industrial areas, farmland, … etc. The characteristics of sub-urban terrain are complex and diverse, including flat terrain, undulating mountains, hills and other terrains, as well as hydrological features, such as rivers and lakes. By analyzing Figure 9, it can be seen that the changes in the shape-factor coefficient curves of the two terrains are similar. In both terrains, the shape coefficients of the roof and leeward surface exceed the specified values in certain wind-direction ranges.

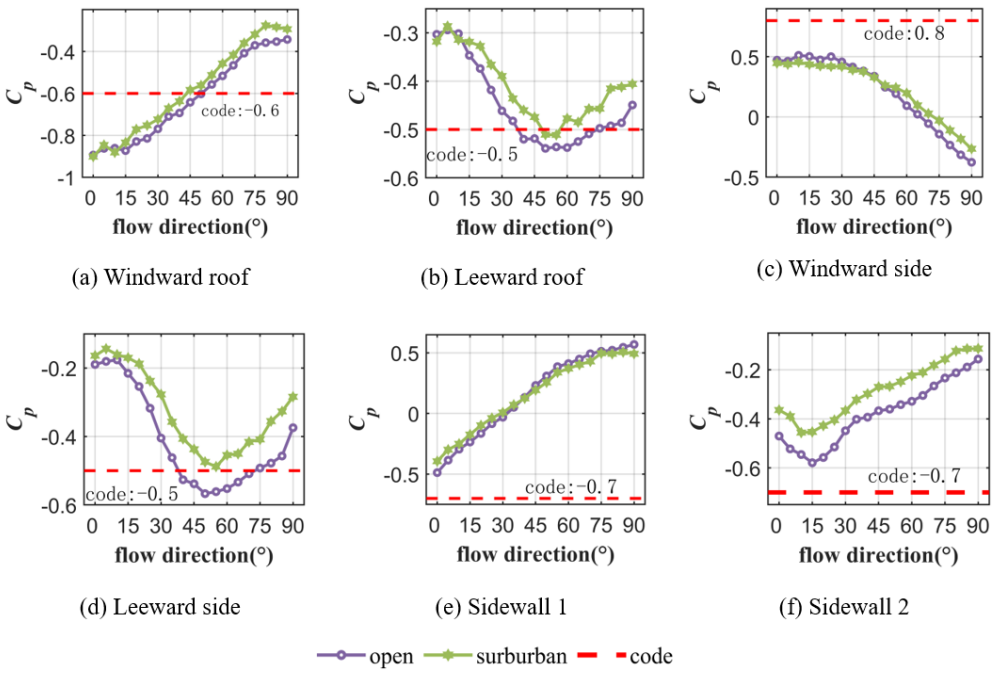

Figure (9): Shape coefficients of each wall under different terrains

Figure 10 displays the wind-pressure distribution on the roof and leeward surface at a wind-direction angle of 50°. For both terrains, the wind-pressure distribution on the roof and leeward surface exhibits similar patterns. The roof experiences a conical vortex, with the maximum negative pressure forming at the windward edge corner, gradually decreasing along the direction of the vortex until it reaches the roof edge. It is recommended to use a form-factor coefficient of -0.5 for the leeward roof and leeward surface of low-rise buildings in sub-urban terrain and -0.6 in open terrain.

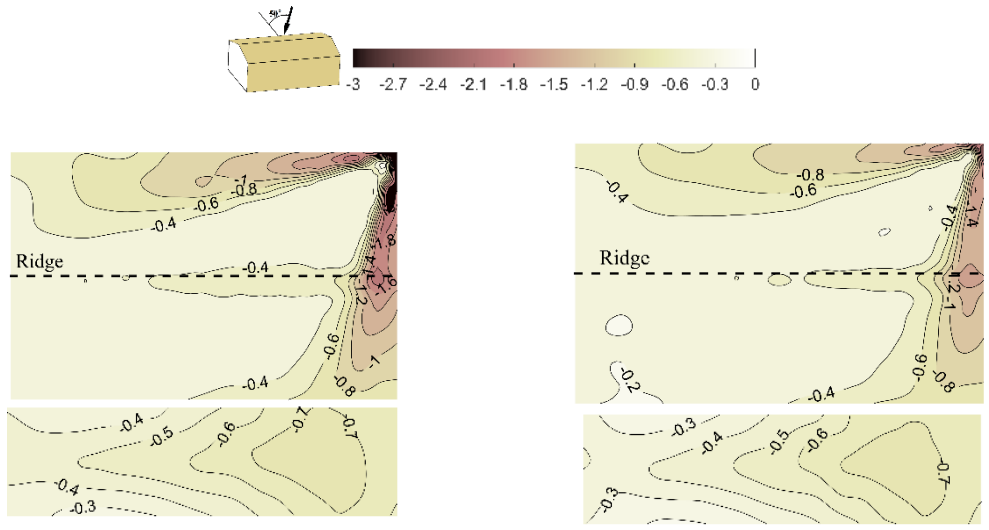

(a) Open terrain; wind-direction angle: 50° (b) sub-urban terrain; wind-direction angle: 50°

Figure (10): Wind-pressure distribution of roof and leeward surface under different terrains

In summary, the shape coefficients for the windward roof, windward facade and sidewall 1 of the building model are similar in different terrains; so, they are not discussed in depth. To summarize, the roof slope, eave height and surrounding-terrain variations all influence the shape coefficients of the building. In certain scenarios, some surface-shape coefficients exceed the prescribed values in the code. Standard values of shape coefficient for windward roofs are -0.6 and -0.6 ~ 0 for slope angles $\alpha \leq 15°$ and $15° < \alpha \leq 30°$, respectively. The standard values are -0.5, -0.7 and -0.5 for the leeward roofs, sidewall 2 and leeward side, respectively. Based on the results of wind-tunnel experiments, the recommended values for the shape coefficients of each building surface are presented in Table 1.

Table 1: Recommended values of shape coefficient for low-rise buildings

Research object		Application condition		Shape coefficient
		Slope angle	Height	
Windward roof	Recommended value	$\alpha \leq 15°$	12.2m	-0.9
		$15° < \alpha \leq 30°$	12.2m	-0.9 ~0
Leeward roof	Recommended value	4.76°	$0 < H \leq 12$m	-0.45~-0.95
		$\alpha \leq 15°$	12.2m	-0.4~-0.75
		$15° < \alpha \leq 30°$	12.2m	-0.75
		4.76°	$H \leq 5$m	-0.4
		4.76°	$5\text{m} < H < 12\text{m}$	-0.4~-0.55
		4.76°	12.2m	-0.6
Sidewall 2	Recommended value	—	12.2m	-0.6
		4.76°	$0 < H \leq 12$m	-0.35~-0.6
		4.76°	12.2m	-0.6
Leeward side	Recommended value	$\alpha \leq 5°$	12.2m	-0.6
		$5° \leq \alpha \leq 30°$	12.2m	-0.6~ -0.4
		4.76°	$H \leq 5$m	-0.4
		4.76°	$5\text{m} \leq H \leq 12\text{m}$	-0.4~-0.6

Note: α is the roof slope angle and H is the eave height. Take a value of ± 0.1 when the absolute value of the body-shape coefficient is less than 0.1. The data in the table shows all recommended values for open terrain.

CONCLUSIONS

Through wind-tunnel numerical experiments, the differences between the form-factor coefficient and the specified values for low-rise buildings were analyzed under different roof slopes, building heights and terrains. Additionally, the influence mechanism of the surrounding flow field on surface-wind pressures was investigated using CFD simulations. The main conclusions are as follows: (1) In buildings with a height of 12.2m and open terrain, for the windward roof, as the roof slope angle increases within 15°, the degree of flow separation and reattachment on the windward roof increases. This leads to larger high negative-pressure areas on the roof, increasing the form-factor coefficient negative values beyond the recommended limit. (2) For buildings with a slope ratio of 1:12 and open terrain, the form-factor coefficient variation curves for different eave heights of the building surfaces show similar trends. Increasing the building height enhances the intensity of vortices around the building, resulting in increased negative pressures on the roof and leeward surface. Under oblique wind conditions, the negative values of the form-factor coefficient exceed the specified limits. (3) Compared to sub-urban terrain, open terrain has reduced ground roughness, resulting in increased intensity of roof cone vortices and leeward-surface wake vortices. This leads to an overall increase in negative pressures on the building surfaces. To conclude, the form-factor coefficients of low-rise buildings are affected by various factors, such as roof slope, building height and terrain, among others. Under certain circumstances, these coefficients may surpass the specified values set by the regulations. Consequently, further refinement is necessary in determining the form-factor coefficients for building surfaces.

Conflict of Interests

The authors declare no conflict of interests.

Data Availability

The raw data supporting the conclusions of this article will be made available by the authors, without undue reservation.

Acknowledgements

This work is supported by Postgraduate Research Innovation Project of Changsha University of Science and Technology (CXCLY2022036).

REFERENCES

Yang, Q., Gao, R., Bai, F. et al. (2018). "Damage to buildings and structures due to recent devastating wind hazards in east Asia". Natural Hazards, 92 (3), 1321-1353.

Huang, B.C., and Wang, C.J. (2008). “The theory of structural wind-resistant analysis and Applications".

Hajra, S., and Dalui, S.K. (2016). "Numerical investigation of wind-load interference effect of square buildings on octagonal tall building". Jordan Journal of Civil Engineering, 10 (4), 462-479.

Yang, W., Quan, Y., Jin, X., Tamura, Y., and Gu, M. (2008). “Influences of equilibrium atmosphere boundary layer and turbulence parameter on wind loads of low-rise buildings". Journal of Wind Engineering and Industrial Aerodynamics, 96 (10-11), 2080-2092.

Yang, L., Gurley, K.R., and Prevatt, D.O. (2013). “Probabilistic modeling of wind pressure on low-rise buildings". Journal of Wind Engineering and Industrial Aerodynamics, 114, 18-26.

Prasad, D., Uliate, T., and Ahmed, M.R. (2009). “Wind loads on low-rise building models with different roof configurations". International Journal of Fluid Mechanics Research, 36 (3).

Cheon, D.J., Kim, Y.C., and Yoon, S.W. (2023). “Fluctuating wind pressure characteristics of dome roofs with low rise-span ratio". Buildings, 13 (7), 1673.

Tariq, A., Singh, J., and Singh, S.K. (2023, February). “Wind-load analysis on gable roof of low-rise building". In: IOP Conference Series: Earth and Environmental Science, 1110 (1), 012093. IOP Publishing.

Irtaza, H., Javed, M.A., and Jameel, A. (2015). “Effect on wind pressures by variation of roof pitch of low-rise hip-roof building". Asian J. Civ. Eng., 16, 869-889.

Ginger J., and Holmes J. (2003). "Effect of building length on wind loads on low-rise buildings with a steep roofs pitch". Journal of Wind Engineering and Industrial Aerodynamics, 91 (11), 1377-1400.

Gu, M., Zhao, Y.L., Huang, Q. et al. (2010). "Wind-tunnel test and numerical simulation of mean wind pressures on roofs of low-rise buildings". Acta Aerodynamica Sinica, 28 (01), 82-87. (in Chinese).

Akon, A.F., and Kopp, G.A. (2016). "Mean-pressure distributions and reattachment lengths for roof-separation bubbles on low-rise buildings". Journal of Wind Engineering and Industrial Aerodynamics, 155, 115-125.

Guo, Y., Wu, C.-H., and Kopp, G.A. (2021). "A method to estimate peak pressures on low-rise building models based on quasi-steady theory and partial turbulence analysis". Journal of Wind Engineering and Industrial Aerodynamics, 218, 104785.

Wang, J., and Kopp, G.A. (2021). "Gust-effect factors for windward walls of rigid buildings with various aspect ratios". Journal of Wind Engineering and Industrial Aerodynamics, 212, 104603.

Kozmar, H. (2020). "Surface pressure on a cubic building exerted by conical vortices". Journal of Fluids and Structures, 92, 102801.

Agrawal, S., Wong, J.K., Song, J. et al. (2022). "Assessment of the aerodynamic performance of unconventional building shapes using 3D steady RANS with SST k-ω turbulence model". Journal of Wind Engineering and Industrial Aerodynamics, 225, 104988.

Xing, F., Mohotti, D., and Chauhan, K. (2018). "Study on localised wind-pressure development in gable-roof buildings having different roof pitches with experiments, RANS and LES simulation models". Building and Environment, 143, 240-257.

Kobayashi, T., Sandberg, M., Fujita, T., Lim, E., and Umemiya, N. (2022). "Numerical analysis of wind-induced natural ventilation for an isolated cubic room with two openings under small mean wind pressure difference". Building and Environment, 226, 109694.

Abdelfatah, N., Elawady, A., Irwin, P. et al. (2022). "Experimental investigation of wind impact on low-rise elevated residences". Engineering Structures, 257, 114096.

Ministry of Housing and Urban-Rural Development of the People's Republic of China. (2012). "GB 50009-2012: Load code for the design of building structures". Beijing: China Architecture and Building Press, (in Chinese).

Ho, T., Surr, D., Morrish, D. et al. (2005). "The UWO contribution to the NIST aerodynamic database for wind loads on low buildings: Part 1. Archiving format and basic aerodynamic data". Journal of Wind Engineering and Industrial Aerodynamics, 93 (1), 1-30.

Ho, T., Surry, D., and Morrish, D. (2003). "NIST/TTU cooperative agreement: Windstorm-mitigation initiative: Wind-tunnel experiments on generic low buildings". London, Canada: BLWTSS20-2003, Boundary-layer Wind-tunnel Laboratory, Univ. of Western Ontario.

Ho, T., Surry, D., and Nywening, M. (2003). "NIST/TTU cooperative agreement: Windstorm-mitigation initiative: Further experiments on generic low buildings". BLWTSS21-2003, Phase 2.

Ming-Fei, C., Chao, X.U., Yu-Ming, L. et al. (2011). "Interpretation of each parameter in wind load standard value calculation formula of load code". Construction & Design for Project, 12 (1), 41-43, 45.

Menter, F.R., Kuntz, M., and Langtry, R. (2003). "Ten years of industrial experience with the SST turbulence model". Turbulence, Heat and Mass Transfer, 4 (1), 625-632.